Matter and Radiation at Extremes | RESEARCH ARTICLE | scitation.org/journal/mre

Large aperture and non-critical phase-matched fourth harmonic generation of Nd:Glass lasers

Cite as: Matter Radiat. Extremes 4, 045401 (2019); doi: 10.1063/1.5087453
Submitted: 1 January 2019 • Accepted: 13 March 2019 •
Published Online: 30 April 2019

Fang Wang, Fuquan Li,[a] Wei Han, Wei Wang, Ping Li, Lidan Zhou,[a] Yong Xiang, Bin Feng, Xuewei Deng, Jingqin Su, and Qihua Zhu

AFFILIATIONS

Research Center of Laser Fusion, China Academy of Engineering Physics, Mianyang 621900, China

[a]Authors to whom correspondence should be addressed: bachangzu@163.com and zhouldpku@gmail.com

ABSTRACT

A fourth harmonic generation (FHG) scheme in focusing beams is proposed and demonstrated for large aperture Nd:glass laser facilities. By placing the focusing lens before the FHG crystal, the problem of ultraviolet damage can be overcome, largely without affecting FHG conversion efficiency owing to the large angular acceptance of the non-critical phase matching technique. A numerical simulation of the FHG process indicates that angular acceptance can be appropriately increased by lowering the working temperature and jointing the two adjacent compensating angles, so that FHG in focusing beams with relatively small F numbers becomes feasible. With a 170 mm × 170 mm × 7 mm and 65% deuterated potassium dihydrogen phosphate crystal mounted in a high-precision, temperature-controlled system, high-efficiency FHG has been demonstrated in the focusing beam with a full beam convergence angle of 36 mrad. When driven with a 223 J, second harmonic radiation (2ω), 1 ns flat-top pulse with a beam area of 130 cm^2, corresponding to 1.7 GW/cm^2 2ω input intensity, 182 J of fourth harmonic radiation (4ω) were generated.

I. INTRODUCTION

In the field of laser-driven inertial confinement fusion (ICF),[1,2] the choice of laser wavelength is one of the most important issues. According to the literature,[3–5] the second harmonic (2ω), the third harmonic (3ω), and the fourth harmonic (4ω) of an Nd: glass laser (1ω) can all be used. However, when choosing the wavelength, both the laser-target coupling and the optics damage should be taken into consideration. In regard to laser-target coupling, the fast electron production process can be suppressed, and the coupling efficiency of a laser with an ignition target can be improved at shorter wavelengths. However, damage to the optical elements becomes worse as wavelength decreases, as the optics damage threshold drops severely when the single-photon energy increases. Concurrently, the gain of nonlinear effects, such as small-scale self-focusing and stimulated scattering, increases dramatically. Therefore, although large aperture fourth harmonic generation (FHG) in potassium dihydrogen phosphate (KDP) crystals with a critical phase matching technique has been previously demonstrated,[6–8] 4ω lights are mostly used in Thomson scattering diagnostic systems,[9–11] where the light energy is not very high. In high-energy and high-power laser systems, for high-energy density physics, such as the National Ignition Facility (NIF),[12,13] Laser Megajoule (LMJ),[14] and SG-III facility,[15] the third harmonic is used rather than the fourth. Nevertheless, recent work[16,17] has shown that achieving laser-target coupling efficiency is challenging owing to plasma instabilities. Therefore, driving the target wholly or partly with high-energy 4ω laser beams is attracting much attention. However, to date, laser facilities are constrained by the UV damage to optics,[18,19] and the damage problem will not be overcome if a standard final optics system is used for 4ω light generation.

Generally, the most serious UV damage to optics occurs at the functional parts of beam focusing and color separation. In NIF and SG-III, this occurs in the wedged focusing lens, and in LMJ, it occurs in the large aperture gratings. Therefore, a solution to this problem is required that reduces the usage of UV optics without affecting the basic functions of the final optical system. Fortunately, owing to its considerable angular acceptance, the non-critical phase matching (NCPM) technique provides such a solution, in which the focusing lens can be placed before the frequency converter. In fact, NCPM FHG in small apertures has recently been reported in deuterated potassium dihydrogen phosphate (DKDP), ammoniumdehydrogen phosphate (ADP) and deuterated ammoniumdehydrogen phosphate (DADP) crystals,[20–24] in which a high efficiency and large angular acceptance

were both demonstrated experimentally. Particularly, the crystals referred to are suitable for large apertures, and their NCPM temperatures are close to room temperature. The above two conditions are beneficial to the application of NCPM FHG in high-energy laser systems. In this paper, we propose a beam-focusing FHG scheme. We describe the basic design and numerical simulations of this scheme; large aperture experiments concerning a focusing beam are also presented.

II. BASIC DESIGN OF BEAM-FOCUSING FHG

The basic scheme of beam-focusing FHG is shown in Fig. 1, in which the focusing lens is placed before the FHG crystal, solving the damage problem of the focusing lens. The conversion efficiency almost remains the same, owing to the large angular acceptance of NCPM technique. Moreover, it is evident from the figure that the 4ω and the residual 2ω focal spots are strictly confocal in the beam-focusing configuration. Based on this arrangement, the target can be driven in three ways with only one final optics assembly. Firstly, for a pure 2ω driving beam, it is necessary only to remove the FHG crystal or to make it totally phase-mismatched by adjusting the angle or temperature, without any other extra modification, even for the focus lens. Secondly, for a pure 4ω driving beam, residual light can be easily dispersed by making the debris shield (DS) a small-angle wedge (about one-sixth the size of a traditional final optics system), as its confocal characteristics make beam separation more efficient, spot-to-spot rather than spot-to-nearfield, along with the much more considerable chromatic aberration in fused silica materials (the refractive index of 2ω, 3ω and 4ω lights in fused silica materials are 1.461, 1.476, and 1.501, respectively[25]). Lastly, the target can be driven by dual-wavelength lasers, which provides a novel and interesting idea for laser-target coupling. In the dual-wavelength driving scheme, the target can be irradiated by 4ω and 2ω lights simultaneously, so that more energy can be coupled to the target, allowing greater focal spot smoothing. Due to the mode mixing mechanism during frequency conversion, the sizes of the 4ω and 2ω focal spots are almost the same, but there are many more high-frequency components in the 4ω spot. As the two spots are completely incoherent, there is room for improvement for the spatial uniformity of target irradiation.

In beam-focusing design, temperature control and F number (defined as the ratio of focal length to beam dimension), parameter optimization is of great importance. First, with respect to the adjustment of non-critical phase matching temperature and temperature uniformity control, the FHG crystal should be mounted in a high-precision thermostat with two windows. We suggest that the thermostat operate in a low vacuum environment (a pressure of about 1 Torr is usually needed to protect the sol-gel coatings of the optics) which maintained by two windows. The window (40 mm thickness)

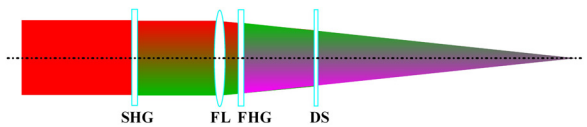

FIG. 1. The basic scheme of beam-focusing FHG design. The fundamental frequency laser is firstly frequency doubled by the second harmonic generation (SHG) crystal and is then focused onto the FHG crystal, so that only the DS is left in the UV segment. FL denotes focusing lens and DS is debris shield.

before the FHG crystal is used as a vacuum window, while the ultraviolet window is used as a separating window whose thickness can be minimized to 10 mm. Therefore, damage problems can be greatly reduced. In addition, to reducing the influence of temperature uniformity on conversion efficiency, a DKDP crystal is adopted as the FHG crystal because of its comparatively larger temperature acceptance compared to that of ADP and DADP crystals.[23] However, although conversion efficiency is less affected with large F number focusing beams, the beam aperture is usually unchangeable, while the focal length of the lens is restricted for the application in a real laser system. Thus, it is essential to optimize the F number and obtain the acceptable limit of the focal length by numerical simulation.

III. NUMERICAL SIMULATIONS

As referred to above, the F number of the focusing beam is the most important parameter in beam-focusing FHG design. To investigate the influence of the F number on the FHG process quantitatively, a numerical model was developed by solving the well-known nonlinear coupled wave equations using a split-step Fourier algorithm.[26] For the purposes of this paper, the self- and cross-phase modulation terms associated with a nonlinear refractive index can be ignored, and the type I doubling process can be expressed as

$$\begin{aligned}\left(\frac{\partial}{\partial z}+\frac{1}{v_{g2}}\frac{\partial}{\partial t}\right)A_2 &= -\frac{i}{2k_2}\nabla_\perp^2 A_2-\frac{1}{2}(\alpha_2+\beta_2|A_2|^2)A_2\\ &\quad+\frac{i\omega_2\chi_{eff}}{n_o(\omega_2,T)c}A_2^* A_4 e^{i\Delta kz},\\ \left(\frac{\partial}{\partial z}+\frac{1}{v_{g4}}\frac{\partial}{\partial t}\right)A_4 &= -\frac{i}{2k_4}\nabla_\perp^2 A_4-\frac{1}{2}(\alpha_4+\beta_4|A_4|^2)A_4\\ &\quad-\rho_4\frac{\partial A_4}{\partial x}+\frac{i\omega_4\chi_{eff}}{2n_e(\omega_4,\theta,T)c}A_2{}^2 e^{-i\Delta kz},\end{aligned} \tag{1}$$

where A_i ($i = 2, 4$) is the complex amplitude, x and y are coordinates in the sensitive and non-sensitive directions of the crystal, z is coordinate in the beam propagation direction, k is the wave vector, ω is the angular frequency, n_o and n_e are the refractive indices for ordinary and extraordinary waves, respectively, c is the speed of light, ρ is the transverse walk-off term of extraordinary waves, v_g is the group velocity, χ_{eff} is the effective nonlinear coefficient, α and β are the linear and nonlinear loss coefficients, respectively, and Δk is the phase matching factor between the two fields, i.e.,

$$\Delta k = \frac{1}{c}[n_e(\omega_4,\theta,T)\omega_4 - 2n_o(\omega_2,T)\omega_2]. \tag{2}$$

The phase matching factor has a direct impact on conversion efficiency, and [see Eq. (2)] it is very sensitive to operating conditions, including crystal temperature, T, and orientation, θ. θ is defined as the angle between the crystal optical axis and the direction of field propagation. For a focusing beam, assuming the beam center is perfectly phase matched, θ is a function of x, and it is inverse proportional to the F number and aperture, D, for a given x, i.e.,

$$\theta(x) = \frac{x}{DF}. \tag{3}$$

The subscripts 2 and 4 denote the parameters for the 2ω beam and 4ω beam, respectively. In the model, the 1ω wavelength is 1053 nm, the effective nonlinearity coefficient of DKDP crystal

is assumed to be 0.46 pm/V, and the two photon absorption (TPA) effect of the 4ω beam is taken into account with a coefficient of 2.7×10^{-11} cm/W,[7] while $\beta_{2\omega}$ is neglected. Linear absorption was neglected because of our findings. The nominal input 2ω intensity was specified as 2 GW/cm^2 to reduce the TPA loss, and the crystal thickness was 7 mm, which is favorable for a high conversion efficiency and an adequate temperature acceptance. The spatial distribution of the input beam was an 8th order super-Gaussian, with a dimension of 360 mm × 360 mm. For simplicity, the temporal profile of the pulse was set to 1 ns flat on top in the simulation.

The influence of incident angle on 2ω–4ω efficiency was studied using the numerical simulation. The angular tuning curve for different working temperatures is shown in Fig. 2. Although the full width at half maximum (FWHM) of the acceptance angle at the NCPM temperature (referred to as T_c, measured to be 29.8 °C for the 65% deuterated DKDP crystal) is about 40 mrad, the flat top area is only 12 mrad, which makes achieving high-efficiency FHG over the entire beam aperture difficult. However, fortunately, when the working temperature is below T_c, phase matching can be achieved by adjusting the incident angle. Therefore, there are two phase-matching angles symmetrically distributed around θ = 90°. By optimizing the working temperature, the two adjacent angles can be jointed, and the angular bandwidth increased.

Based on our findings, we calculated the evolution of the 2ω–4ω efficiency vs the F number for different working temperatures, as shown in Fig. 3. Conversion efficiency increases as the F number increases, and then gradually tends to a constant value equivalent to that in the collimated beam. The degradation of efficiency at smaller F numbers is caused by the relatively large detuned angle at the edge of the focusing beam, expressed by Eq. (3). When the working temperature is higher than T_c, the efficiency curve is always less than that at T_c. But when the working temperature is lower than T_c, conversion efficiency before the inflection point can be better than that under NCPM conditions. This result is in accordance with the viewpoint described above.

The inset pictures of Fig. 3 show the 4ω near-field distribution at different F numbers, where $F = 50$ represents the flat top area of the curve, $F = 28$ is about the inflection points of the curves, and $F = 10$ represents the half maximum position. Evidently, the near-field along the insensitive axis of the DKDP crystal is almost unaffected in all cases, as the conversion efficiency is non-sensitive to the incident angle in this direction. But in the sensitive axis direction, the degradation turns more and more severely as the F number becomes smaller. The near-field is not affected by an F number of 50. However, for $F = 28$, where the inflection point appears, degradation on the edge of the near-field along the X axis is apparent. Furthermore, for $F = 10$, the near-field from the center to the edge at first collapses and then slightly rebounds, as the secondary peaks of the efficiency-angle tuning curve begin to become important. This can also explain the evident kinks appearing in the curves.

The focal length for $F = 28$ is close to the limit for real facilities; therefore, we attempted to optimize the working temperature to achieve a higher efficiency and better beam uniformity. Figure 4 shows the calculated 2ω–4ω efficiency curves vs working temperature and focusing beam at $F = 28$; the tuning curve for the collimated beam is also shown for comparison. The maximum conversion efficiency for the focusing beam at $F = 28$ is achieved when the working temperature is 0.2 °C lower than T_c, which can obtain an increase of 3.5% in comparison with the non-compensation scenario ($T = T_c$). Although the maximum conversion efficiency is 3% compared to that of the collimated beam, a good compensation is realized around the perimeter of the near-field, which can be seen in Fig. 5.

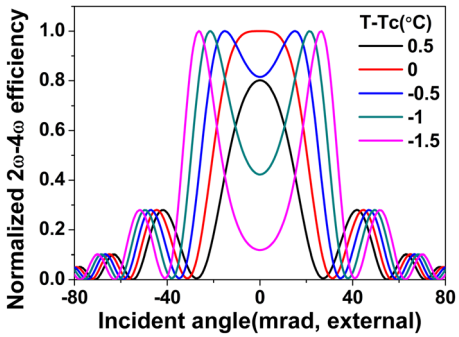

FIG. 2. Normalized 2ω–4ω efficiency curves vs beam incident angle at different working temperatures. The curves show the complementary relationship of angle and temperature in the phase matching condition.

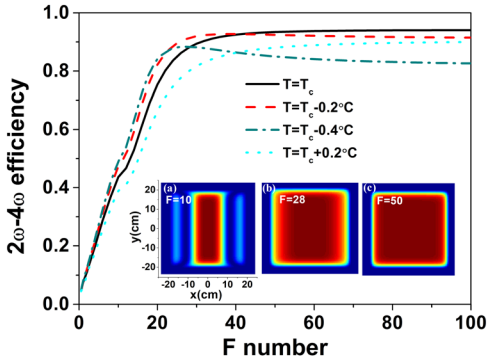

FIG. 3. Calculated 2ω–4ω efficiency vs F number of the focusing beam at different working temperatures. The insets show 4ω near-field evolution with an F number of (a) 10, (b) 28, and (c) 50 when the DKDP crystal is working at T_c.

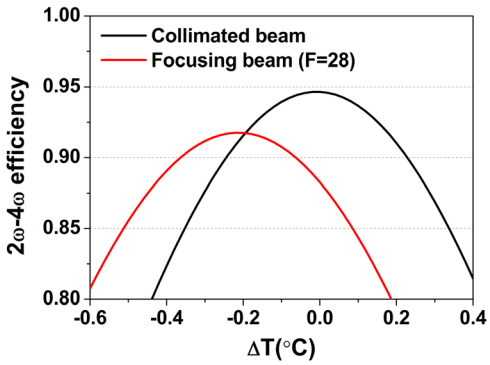

FIG. 4. Calculated 2ω–4ω efficiency curves vs working temperature for a collimated beam and focusing beam at $F = 28$. The maximum efficiency of the focusing beam is achieved when the working temperature is 0.2 °C lower than T_c. An increase of 3.5% can be achieved after compensation.

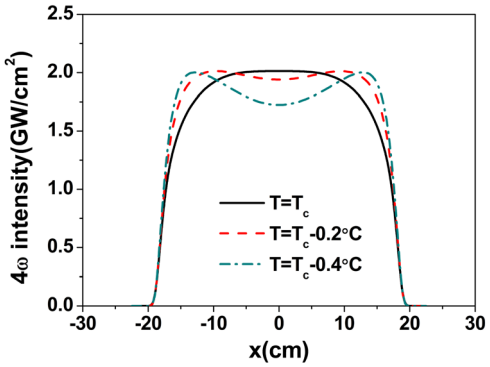

FIG. 5. The distribution of 4ω near-field in the center section of the non-sensitive direction (y = 0) with different working temperatures for $F = 28$. When the working temperature is 0.2 °C lower than T_c; however, the overall efficiency is 3% lower than in the collimated beam; the near-field at the perimeter is satisfactory.

IV. LARGE APERTURE FHG EXPERIMENTS

To verify the beam-focusing FHG scheme, including high-efficiency FHG in a focusing beam and damage resistance of the FHG crystal, large aperture experiments were performed. The experimental layout is shown in Fig. 6(a). To achieve high efficiency and high beam quality with the 4ω laser, the DKDP crystal uniformity and temperature across the crystal should be considered for large aperture FHG experiments. A conventionally grown and 65% deuterated DKDP crystal with dimensions of 170 mm × 170 mm × 7 mm was prepared to achieve NCPM FHG, near room temperature. The DKDP crystal was cut for type I (ooe) phase matching, with the incident 2ω beam propagating perpendicularly to the crystal Z axis (θ = 90°) and at 45° to the crystal X axis (ϕ = 45°). The input and output surfaces of the DKDP crystal were anti-reflection coated for the 2ω and 4ω light, respectively.

The FHG crystal was mounted in a high-precision temperature control system [see Fig. 6(b)], in which temperature uniformity across the crystal was controlled to within 0.1 °C (peak-to-valley value). The dimensions of the system were 1000 mm × 340 mm × 340 mm and the temperature could be changed from 10 °C to 40 °C. Inside the system, the crystal was located in a vacuum and two deep-ultraviolet fused silica windows were situated at both ends of the system to isolate the atmosphere. There were three layers to provide uniform temperature control for the crystal. The one furthest inside was a stainless-steel crystal frame with constant-temperature recycling water, and its surface was processed to be less than 5 μm from peak-to-valley to provide the desired contact area of the crystal. The middle layer was composed of a dense constant-temperature water loop attached to the walls of the stainless-steel cavity, and the outside layer was made of heat insulation materials. Owing to the symmetrical structure of the temperature control chamber and the vacuum environment, with no heat conduction, the temperature distribution over the crystal was symmetrical.

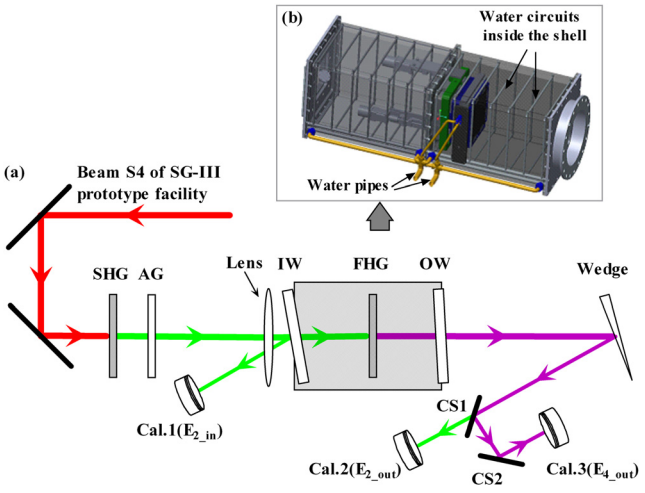

FIG. 6. (a) Experimental layout of large-aperture NCPM FHG in the focusing beam. (b) Schematic of the thermostat.

The experiment was carried out on the SG-III prototype facility, and one of the eight beams was introduced into the FHG experimental platform by three high-reflection mirrors. The 1ω beam had a narrow bandwidth and a flat-top pulse shape with a pulse duration of 1 ns at a wavelength of 1053 nm. The spectral bandwidth was about 6 pm FWHM. The beam size was limited to 140 mm × 140 mm using a liquid crystal light valve, and the spatial distribution was approximately an 8th order super-Gaussian. As shown in Fig. 6, the 1ω beam passes through the SHG crystal, absorbing glass (AG), focusing lens, input window (IW), FHG crystal, output window (OW), and Wedge, in sequence. The SHG crystal was a 16-mm thick type I KDP crystal, and the AG was used to absorb the residual 1ω beam. The focal length of the lens was 3.9 m, so that the full beam divergence angle was 36 mrad and the F number of the focusing beam was 28, which was in accordance with the numerical simulation. The FHG crystal was located 72 cm away from the lens; thus, the beam size on the crystal was converged to 113 mm × 113 mm. Both the input and output windows were uncoated to avoid possible damage. The input window was fixed at a tilt angle of 10° for the 2ω beam energy sampling measurement. The generated 4ω light and the residual 2ω light were sampled with an uncoated wedge, and separated by two color separators (CS1 and CS2), and then measured with two calorimeters (Cal.2 and Cal.3), respectively. The NCPM FHG experiment using a collimated beam can also be conducted with the experimental layout shown in Fig. 6, but by removing the lens and replacing the Wedge with a concave mirror.

The temperature tuning curves of FHG with the collimated beam and the focusing beam are shown in Fig. 7. The black squares refer to the experimental results with the collimated beam while the red solid circles denote beam-focusing FHG; both results were obtained when the input 2ω intensity was 0.5G W/cm^2. For comparison, the calculated FHG temperature tuning curves are also presented in Fig. 7. As indicated by the results, the non-critical phase matching temperature is 29.8 °C with a temperature acceptance bandwidth of 3.1 °C (FWHM). The optimal working temperature of beam-focusing FHG is 0.2 °C lower than that in NCPM FHG with the collimated beam, but the temperature acceptance bandwidth is almost the same as that of the collimated beam. This is in accordance with the numerical prediction referred to above.

Efficient FHG was obtained in the focusing beam with a crystal temperature of 29.6 °C. Figure 8 shows the measured 2ω–4ω

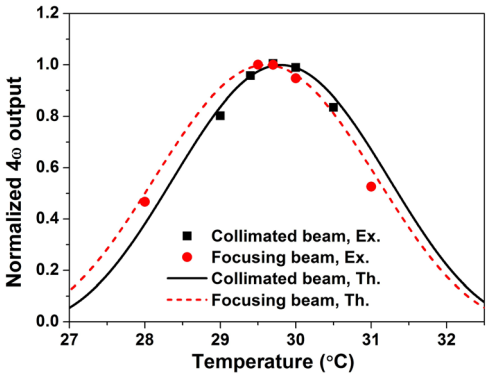

FIG. 7. Measured temperature tuning curves for FHG in a 65% deuterated DKDP crystal with the collimated beam (black squares) and focusing beam (red circles). The black solid curve and red dashed curve correspond to the calculated results.

conversion efficiency and the output 4ω energy as functions of input 2ω intensity; the calculated results are also given in Fig. 8 with solid curves for comparison. A maximum 4ω energy of 182 J is generated with an input 2ω energy of 223 J, corresponding to a conversion efficiency of 81.6%. The highest 4ω flux was 1.4 J/cm^2/1 ns. The TPA effect is not prominent possibly because it is self-consistent with the measured energy balance results (defined as E_4_out plus E_2_out divided by E_2_in). After more than twenty shots, crystal damage was examined using a dark field image, which did not show any evident surface damage, except for several individual pinpoints and some dust around the beam area. The transmissivity was measured after the experiment and remained the same as before.

Furthermore, as high-power laser facilities usually use a smoothing technique with spectral broadband, the bandwidth acceptance of the FHG process should be of concern. Due to high dispersion in the UV band, the FHG process is very spectrally sensitive. As the blue circles in Fig. 8 show, with 1ω bandwidth of 0.3 nm, 2ω–4ω efficiency drops rapidly as input intensity grows, meaning it would jar with the SSD (smoothing by spectral dispersion) technique. If needed, a new beam smoothing technique we proposed recently may solve this problem. The technique is based on ultra-fast angle sweeping with narrowband pulses. Moreover, by using the dual-wavelength lasers driving scheme, conversion efficiency becomes less important, meaning this problem can be overcome.

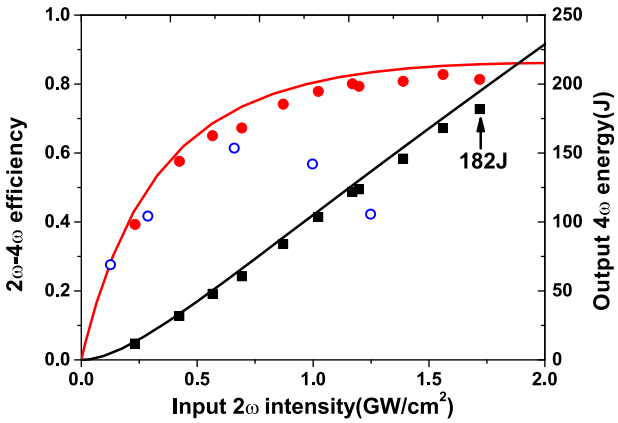

FIG. 8. Measured 2ω–4ω efficiency (red circles) and output 4ω energy (black squares) plotted as a function of input 2ω intensity. Solid curves are calculations for comparison. The blue circles denote the measured FHG efficiency with a 1ω bandwidth of 0.3 nm.

V. SUMMARY

In conclusion, we have proposed a beam-focusing FHG design, in which the focusing lens is placed before the FHG crystal to obviate the UV damage inflicted on large aperture high-energy laser facilities. The FHG conversion efficiency of this scheme is almost unaffected owing to the large angular acceptance of NCPM. A numerical simulation of the FHG process was conducted by solving nonlinear coupled wave equations, which indicates that angular acceptance can be appropriately increased by lowering the working temperature and jointing the two adjacent compensating angles, so that the focusing beam, with relatively small *F* numbers, becomes feasible. In our study, with 2ω intensity, 2 GW/cm^2 and a DKDP crystal thickness of 7 mm, the *F* number acceptance limit is about 28. A large aperture FHG experiment has been demonstrated in the focusing beam with a full beam divergence angle of 36 mrad. The results show that a 4ω energy of 182 J and 2ω–4ω conversion efficiency of 82% were obtained.

ACKNOWLEDGMENTS

This work was supported by the National Natural Science Foundation of China under Grant Nos. 11704352 and 61775199. The large aperture DKDP crystal was provided by State Key Laboratory of Crystal Materials, Shandong University. The authors would like to express thanks to the operation group of the SG-III Prototype Facility for laser operation and experimental supports.

REFERENCES

[1]E. M. Campbell, "The physics of megajoule, large-scale, and ultrafast short-scale laser plasmas," Phys. Fluids B **4**(11), 3781–3799 (1992).
[2]K. Lan, J. Liu, Z. Li, X. Xie, W. Huo *et al.*, "Progress in octahedral spherical hohlraum study," Matter Radiat. Extremes **1**(1), 8–27 (2016).
[3]H. Nishimura, H. Azechi, K. Yamada, A. Tamura, Y. Inada *et al.*, "Experimental study of wavelength dependences of laser-plasma coupling, transport, and ablation processes," Phys. Rev. A **23**(4), 2011–2019 (1981).
[4]C. Garban-Labaune, E. Fabre, C. E. Max, R. Fabbro, F. Amiranoff *et al.*, "Effect of laser wavelength and pulse duration on laser-light absorption and back reflection," Phys. Rev. Lett. **48**(15), 1018–1021 (1982).
[5]Y. Li, C. Zhai, G. Ren, J. Gu, W. Huo *et al.*, "P2 asymmetry of Au's M-band flux and its smoothing effect due to high-Z ablator dopants," Matter Radiat. Extremes **2**(2), 69–76 (2017).
[6]I. A. Begishev, A. A. Gulamov, E. A. Erofeev *et al.*, "The limiting efficiency harmonics generation of neodimium laser radiation," Izvestiya AN SSSR **47**(10), 1910–1918 (1983).
[7]G. J. Linford, B. C. Johnson, J. S. Hildum *et al.*, "Large aperture harmonic conversion experiments at Lawrence Livermore national laboratory," Appl. Opt. **21**(20), 3633–3643 (1982).
[8]D. Bruneau, A. M. Tournade, and E. Fabre, "Fourth harmonic generation of a large-aperture Nd:glass laser," Appl. Opt. **24**(22), 3740–3745 (1985).
[9]S. H. Glenzer, T. L. Weiland, J. Bower, A. J. MacKinnon, and B. J. MacGowan, "High-energy 4ω probe laser for laser-plasma experiments at Nova," Rev. Sci. Instrum. **70**(1), 1089 (1999).

[10]J. Mackinnon, S. Shiromizu, G. Antonini, J. Auerbach, K. Haney *et al.*, "Implementation of a high energy 4ω probe beam on the Omega laser," Rev. Sci. Instrum. **75**(10), 3906–3908 (2004).

[11]J. S. Ross, J. L. Kline, S. Yang, M. Henesian, T. Weiland *et al.*, "4ω Thomson scattering probe for high-density plasma characterization at Titan," Rev. Sci. Instrum. **81**(10), 10D524 (2010).

[12]P. Wegner, J. Auerbach, T. Biesiada, S. Dixit, J. Lawson *et al.*, "NIF final optics system: Frequency conversion and beam conditioning," Proc. SPIE **5341**, 180–189 (2004).

[13]A. Haynam, P. J. Wegner, J. M. Auerbach, M. W. Bowers, S. N. Dixit *et al.*, "National Ignition Facility laser performance status," Appl. Opt. **46**(16), 3276–3303 (2007).

[14]J. Miquel, C. Lion, and P. Vivini, "The LMJ program: Overview and status of LMJ & PETAL projects," in *CLEO: 2013, OSA Technical Digest (Online)* (Optical Society of America, 2013), paper no. ATu1M.4.

[15]W. Zheng, X. Wei, Q. Zhu, F. Jing, X. Hu *et al.*, "Laser performance upgrade for precise ICF experiment in SG-III laser facility," Matter Radiat. Extremes **2**(5), 243–255 (2017).

[16]M. J. Edwards, P. K. Patel, J. D. Lind, L. J. Atherton, S. H. Glenzer *et al.*, "Progress towards ignition on the National Ignition Facility," Phys. Plasmas **20**(7), 070501 (2013).

[17]H. S. Park, O. A. Hurricane, D. A. Callahan, D. T. Casey, E. L. Dewald *et al.*, "High-adiabat high-foot inertial confinement fusion implosion experiments on the National Ignition Facility," Phys. Rev. Lett. **112**(5), 055001 (2014).

[18]B. Bertussi, P. Cormont, S. Palmier, P. Legros, and J. L. Rullier, "Initiation of laser-induced damage sites in fused silica optical components," Opt. Express **17**(14), 11469–11479 (2009).

[19]X. Gao, G. Y. Feng, J. H. Han, and L. L. Zhai, "Investigation of laser-induced damage by various initiators on the subsurface of fused silica," Opt. Express **20**(20), 22095–22101 (2012).

[20]S. T. Yang, M. A. Henesian, T. L. Weiland, J. L. Vickers, R. L. Luthi *et al.*, "Noncritically phase-matched fourth harmonic generation of Nd:glass lasers in partially deuterated KDP crystals," Opt. Lett. **36**(10), 1824–1826 (2011).

[21]S. Ji, S. Zhang, M. Xu, B. Liu, L. Zhu *et al.*, "Non-critical phase-matching conditions for fourth harmonic generation of DKDP crystal," Opt. Mater. Express **2**(6), 735–739 (2012).

[22]S. Ji, F. Wang, L. Zhu, X. Xu, Z. Wang *et al.*, "Non-critical phase-matching fourth harmonic generation of a 1053-nm laser in an ADP crystal," Sci. Rep. **3**, 1605 (2013).

[23]F. Wang, F. Li, X. Chai, L. Wang, W. Han *et al.*, "Efficient fourth harmonic generation of Nd:glass lasers in ADP and DKDP crystals," Proc. SPIE **9255**, 92551R (2015).

[24]S. Ji, F. Wang, M. Xu, L. Zhu, X. Xu *et al.*, "Room temperature, high-efficiency, noncritical phase-matching fourth harmonic generation in partially deuterated ADP crystal," Opt. Lett. **38**(10), 1679–1681 (2013).

[25]H. Malitson, "Interspecimen comparison of the refractive index of fused silica," J. Opt. Soc. Am. **55**(10), 1205 (1965).

[26]P. J. Wegner, J. M. Auerbach, C. E. Barker, S. C. Burkhart, S. A. Couture *et al.*, "Frequency converter development for the National Ignition Facility," Proc. SPIE **3492**, 392–405 (1999).